

Ab-initio study of tuning the electronic and magnetic properties of Ni₂MnGa Heusler alloy by Co and Mn compound doping

Karunakaran M and Rudra Banerjee

Department of Physics and Nanotechnology, SRM Institute of Science and Technology, Kattankulathur, Tamil Nadu, 603203, India

January 31, 2023

Abstract

We report the effects of Mn and Co doping on the electronic properties, magnetic exchange interaction, and Curie temperature of intermetallic Ni₂MnGa by Green's function based Korringa-Kohn-Rostoker method with coherent potential approximation (KKR-CPA). The effect of single and compound doping of Mn and Co at different crystallographic positions on these properties are evaluated by computing the electronic and magnetic structures of Ni₂MnGa. The study revealed the possibility of tuning magnetic exchange interaction (\mathcal{J}_{ij}) and Curie temperature (T_C) upon doping. Moreover, it is noted that doping can stabilize the Jahn-Teller distortion. It is also worth noting that T_C responds in a different way with concentration as well as the site of the dopant. This study helps in understanding and realizing the cause for magnetic properties in Ni₂MnGa, and experimental peers can also use it for further research on doped Ni₂MnGa.

1 Introduction

Energy is the necessary evil of the modern civilization. Reducing the production of greenhouse gas while keeping on with the ever-increasing energy demand is a great challenge to mankind. Renewable energy technologies are one of the most trusted and tested methods to limit greenhouse emissions and global warming. For caloric materials, which is one of the

major parts of renewable energy, the efficiency depends on ordering temperature, e.g., Curie temperature(T_C) for magnetocaloric (MC) materials. Hence, to achieve the goal of 4/5th of the world's electricity by 2050 [1] from renewable sources, it is extremely important to be able to tune the T_C of the related materials [2].

Since the theoretical prediction of half-metallic properties in NiMnSb by Groot [3] and experimental observations by [4, 5, 6], Heusler alloys(HA's) have drawn massive attention from the scientific community [7, 8, 9] ascribed to their wide usage in MC devices [10], magnetic shape memory alloys [11], spintronics [12], and giant magnetoresistance devices [13, 14, 15]. The full HA's, with generic symbol X_2YZ stabilizes in the $L2_1$ structure [16] with a completely ordered phase. The $Y - Z$ disordered structure has the B_2 ground state [17], while the complete $X - Y - Z$ disordered system has the A_2 [18]. Wyckoff positions of $4a(0, 0, 0)$, $4b(\frac{1}{2}, \frac{1}{2}, \frac{1}{2})$, and $8c(\frac{1}{4}, \frac{1}{4}, \frac{1}{4})$ are occupied by Z , Y , and X , respectively [11, 19, 20]. The ternary full HA, Ni₂MnGa, exhibits both magnetic and structural phase transition [21]. In this context, Ni-Mn-Ga systems show properties like shape memory effect and magnetic field-induced strain, which is advantageous in actuators and sensors [11, 22]. They also show favorable MC (both conventional and inverse) properties, suitable to replace the century-old Joule-Thomson cooling [23, 24]. Ni-Mn-Ga system exhibits magneto structural phase transition with a huge change in isothermal magnetic entropy($\Delta S_m \approx -18 \text{ J kg}^{-1} \text{ K}^{-1}$) but a relatively narrow range of working temperature in full-width half maximum(T_{fwhm}) around 290 K for an applied field change of 5 T, typical to the materials with first-order phase transition(FOPT) [25]. However, the thermal hysteresis of FOPT and the Curie temperature is predominant to magnetic refrigeration.

The electronic structure and magnetic properties have been reported for Ni-doped Co₂MnAl [26] and Co-doped Ni₂MnAl [27] systems, with the dopant at the X position only. Off-stoichiometric Ni_{2-x}Q_xMnGa and Ni_{2-x}Q_xMnGa_{1-z}R_z, where Q, and R are the dopant elements. For the past few decades, Ni_{2-x}Q_xMnGa/Al has been under study to understand their martensite phase transition(T_M) and Curie temperature(T_C) [28, 29]. In Ni_{2+x}Mn_{1-x}Ga, observed that the MC effect is the highest around $0.18 \leq x \leq 0.27$ concentration as magnetic and structural phase change occurs in this region [30]. Partially substituting Ni with Co is generally known to enhance the ferromagnetic coupling and hence the T_C . This increases the possibility that the quaternary system undergoes a martensitic transition together with a meta-magnetic phase transition [31].

Generally, the structural and magnetic properties are highly impacted by the off-stoichiometric combination of the main group element(Z) and transition metals(X and Y). The effect of Y replacing Z , mostly Ni₂MnZ_{1-y}Mn, $Z = \text{Ga, In, etc.}$, is well studied [14, 32, 33]. Substituting the Mn element in the Z position can stabilize the cubic state of the system [14]. The Mn_Z atoms interact antiferromagnetically between the surrounding Mn_Z and normal Mn_Y since the distance between Mn_Y-Mn_Z is shorter than Mn_Y-Mn_Y and Mn_Z-Mn_Z [34]. Here, Mn_Z

has been denoting the Mn atom in the Ga site(Z), and Mn_Y is the Mn's normal position(Y). The doping of the Co element in the X position can increase the ferromagnetic interaction between the atoms and the Curie temperature of the material [31]. Additionally, even a small concentration of Co atoms in the X position significantly impacts the Curie temperature. Also, the cell volume effect and valence electron concentration per atom ratio(e/a) affect T_C inversely, i.e., as the e/a ratio increases, the T_C decreases and vice-versa [35, 36].

From the above discussion, investigation of the effect of doping both the X and the Z sites with d elements, resulting to a disordered $Ni_{2-x}Co_xMnGa_{1-z}Mn_z$, is interesting due to site preferences and their compound effect of electronic, magnetic, and thermodynamic properties. We have investigated the effect of Co and Mn in the X and Z site and observed the effect in a restricted cubic phase. The cubic phase has minimum energy in the $L2_1$ structure. Increasing the Co concentration above 10% retains the cubic state as the ground state in a $B2$ structure [37]. At around $x = 0.25$, the cubic (austenite) phase collapses to the tetragonal (martensitic) phase[27]. We expected Mn doping in the Ga site and Co doping in the Ni site to enhance the material's magnetic moment and Curie temperature. The x concentration varies from a value greater than 10%, i.e., $x = 0.12$ to 0.24. Additionally, the z concentration varies from 0 to 0.5 since the e/a ratio increases up to 8, comparatively for the pure system $Ni_2MnGa(e/a = 7.5)$. Therefore, the z concentration is up to 0.5. This disorder system will be referred to as $NiMnGa(x, z)$ hereafter, where x, z is the concentration of Co in the Ni site and Mn in the Ga site, respectively, for brevity. For example, $Ni_{1.88}Co_{0.12}MnGa_{0.74}Mn_{0.26}$ will be denoted as $NiMnGa(0.12, 0.26)$.

Notably, in this work, we have reported systematic studies of the variation of electronic structure, magnetic exchange interactions, and tuning the Curie temperature(T_C) of this disordered $NiMnGa(x, z)$ system. We have especially looked into patterns of the effect of variation of site occupancy upon a specific substitution for a wide range of concentrations. The results are interpreted from the outcome of electronic structure calculations. This approach enables us to understand the microscopic origin of the macroscopic property(T_C). The study of the substitution of a single $3d$ element on Ni_2MnGa is, as discussed above, very scattered. The investigation of double doping in Ni_2MnGa is rare and far between. However, they offer exciting phenomena, not only from the perspective of fundamental understanding but also for materials engineering with target properties. For example, the tuning of T_C is technologically relevant as it is one of the crucial factors that act as the working temperature range of many devices, namely, MC, spintronics, etc. [10, 12].

2 Methods

The appropriate method for handling off-stoichiometric compositions is Green's function-based formalism with coherent potential approximation(CPA), as in the case of $Ni_{2-x}Q_xMnGa_{1-z}R_z$ [38].

We have performed *ab-initio* calculations using multiple scattering Green's function formalism as implemented in spin polarised relativistic Korringa-Kohn-Rostoker (SPRKKR) code [39, 40, 41]. The Perdew-Burke-Ernzerhof within generalized gradient approximation is used as the exchange-correlation functional [42]. First Brillouin zone integrations were performed with 2500 grids of k -points, and energy convergence criteria were set as 10^{-5} Ry in the calculation in the range. We have implemented full potential spin-polarized scalar relativistic implementation of SPRKKR with angular momentum cut-off $\ell_{max} = 2$ as suitable for our system.

The lattice parameter with a minimum energy of NiMnGa(x, z) is calculated using the following procedure: (i) Obtain the lattice parameter from the materials project database [43]; (ii) Calculated the self-consistent field of the system, with varying lattice parameter ranging from 94% to 106%, with identical calculation for each lattice parameters. (iii) Fit the lattice parameter vs energy plot obtained in the last step using a 4th order polynomial. The parameter corresponding to the minima of the curve is the optimized lattice parameter. For NiMnGa(x, z), we have taken the optimized lattice parameter of previous calculations that has a minimum x, z change as the starting point and followed the steps above. We have shown the optimization curve of NiMnGa(0, 0) in Figure (1a). Other minimization energy curves are not shown here for brevity. In the present study, doping concentrations are varied by changing the Wyckoff site occupancy of the corresponding element in the input structure. The resultant structure is used for further calculations.

The magnetic exchange energy ($\mathcal{J}_{ij}^{\nu\mu}$) was calculated to understand the properties of magnetic interactions. The Heisenberg model is defined as,

$$H = \sum_{\nu,\mu} \sum_{i,j} \mathcal{J}_{ij}^{\nu\mu} \mathbf{e}_i^\nu \cdot \mathbf{e}_j^\mu \quad (1)$$

where ν, μ represent atoms in different sublattices, i, j is a different lattice point, \mathbf{e}_i^ν is the magnetic orientation of i^{th} atom at ν sublattices. The $\mathcal{J}_{i,j}^{\nu\mu}$ is calculated by the energy difference due to an infinitesimal change of magnetic direction, as formulated by Lichtenstein [44].

Finally, the T_C is estimated using mean field theory, yielding

$$k_B T_C = \frac{3}{2} \mathcal{J}_l^{\nu\mu} \quad (2)$$

where \mathcal{J}_l is the largest eigenvalue of the determinant, as described in [34]. It must be remembered that mean field calculations generally overestimate the T_C .

3 Results

We have calculated the electronic and magnetic properties of $\text{NiMnGa}(x, z)$ for ($x = 0.0, 0.12$ and 0.24) and ($z = 0.0, 0.15, 0.26, 0.35$ and 0.5). The optimized lattice parameter of each sample was calculated using the method described in the sec. (2) and tabulated in Tables (1, 2, 3). Figure (1d) shows the variation of lattice parameters with x and z , which is mostly linear.

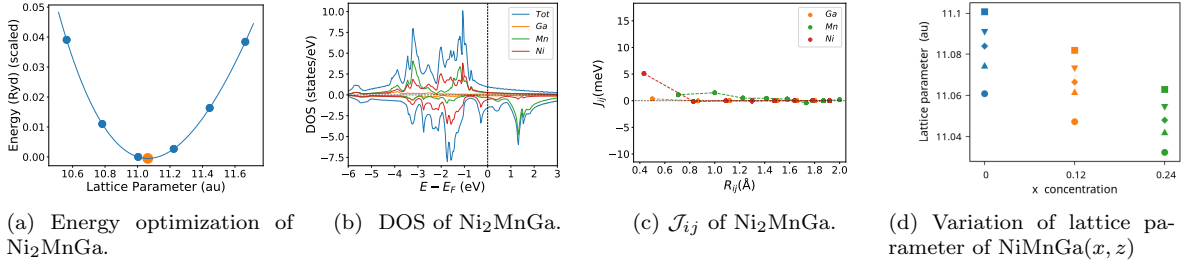


Figure 1: Structure, electronic and magnetic properties of Ni_2MnGa . Figure (1a) shows the energy/volume optimization of Ni_2MnGa . The blue dots are the actual calculation points; the orange dot is the lattice parameter for minimal energy. Figure (1b) and Figure (1c) shows the total and atoms projected DOS and magnetic pair interactions respectively. Figure (1d) shows the variation of lattice parameters as a function of doping concentration at the X and Z sites. Here, the symbol's colors blue, orange, and green represent the values of $x = 0, 0.12$, and 0.24 . The filled symbols of circle, upward triangle, diamond, downward triangle, and square are indicating the $z = 0, 0.15, 0.26, 0.35$, and 0.50 , respectively.

Figures (1a-1c) shows the calculations of the pure Ni_2MnGa . Figure (1a) shows the lattice parameter optimization as described in section (2). Our calculated density of states(DOS) (Figure (1b)) and magnetic exchange interactions(\mathcal{J}_{ij}) (Figure (1c)) with the Mn atom at the center for Ni_2MnGa matches the previous findings [45]. The \mathcal{J}_{ij} is highest for Ni-Mn interactions, with the value ≈ 5 meV. All the interactions are predominantly ferromagnetic in this case. The complete table of optimized lattice parameters, the total and individual magnetic moment per atom, and Curie temperature of the pure system is tabulated in Table (1).

The change of lattice parameter with x, z in the cubic domain is shown in Figure (1d). This trend shows that doping Co at the X site decreases the lattice parameter but doping at the Z site increases the lattice parameter.

3.1 $\text{NiMnGa}(x, 0)$ systems

The $\text{NiMnGa}(x, 0)$ system, doping in Ni site only, though heavily studied within the austenite phase, we have included them for completeness. The doping of Co in the X position will decrease the lattice parameter of the material shown in Figure (1d) and Table (1). The electronic and magnetic structures of $\text{NiMnGa}(x, 0)$ are shown in Figure (2) as representative

of the series. Generally, the X and Y site atoms contribute more to the net magnetic moment of the system. Here the Mn atom loses the moment due to the presence of an effective X site(Ni with Co), and the Ni atom holds the magnetic moment up to the other elements present with the Ni atom. While replacing the Ni with Co in the X site, the moment of Ni increases up to 14% for $z = 0.12$ and 0.24 , as tabulated in Table (1). The Co atom has a much higher magnetic moment($\approx 1 \mu_B$) than Ni($\approx 0.3 \mu_B$), and the \mathcal{J}_{ij} is also much higher than Ni_2MnGa . Increasing the Co concentration causes the magnetic moments of Co and Mn to start decreasing, and the magnetic moment of Ni starts increasing, thereby enhancing the total magnetic moment of the system. Of course, in the current case, $\text{Mn}_Z = 0$.

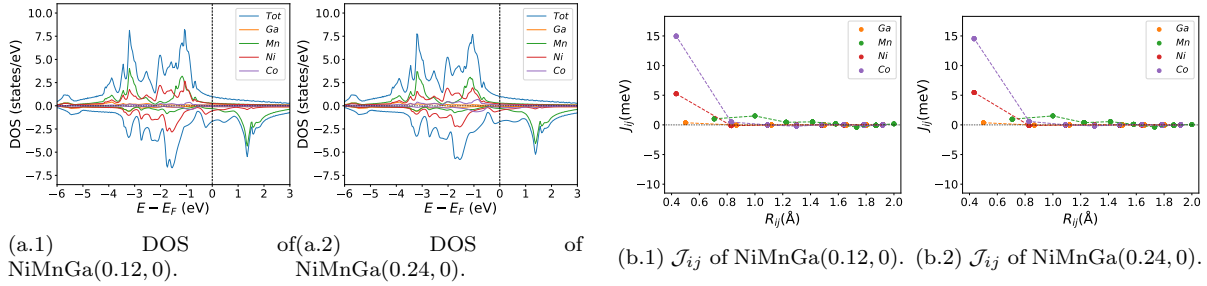


Figure 2: The (a)DOS and (b)exchange interaction of $\text{NiMnGa}(x, 0)$ with $x = 0.12$ in Figure (a.1,b.1) and $x = 0.24$ in Figure (a.2,b.2). Compared to DOS of pure $\text{NiMnGa}(0, 0)$, (Figure (1b)), the DOS shows smeared peak just below the Fermi level and shrank pseudogap in minority spin channel with increase in x . Figure (b) shows the magnetic exchange interaction with the Mn_Y atom at the center. The magnetic interaction remains almost the same between $x = 0.12$ and $x = 0.24$ with the largest interaction between the Co and Mn.

The magnetic properties depend substantially on the exchange interactions between all pairs of chemical elements. In Figures (1c), (2b.1), (2b.2), the exchange interaction is shown for each atom in the configuration of $x = 0, 0.12$, and 0.24 , and $z = 0$. From these Figures, the interactions between all pairs(Ni-Mn, Co-Mn, Mn-Mn, and Ga-Mn) are ferromagnetic, and especially the Ni-Mn and Co-Mn are more ferromagnetic. The interaction between Ni/Co and Mn atoms in different sublattices is consistently ferromagnetic [46]. In this way, the replacement of Ni with Co in the X site enhanced the exchange interaction energy in Co-Mn pair, then the ferromagnetic coupling also increased. These enhanced ferromagnetic coupling caused an increase in the Curie temperature of the material. The pair of exchange coupling of Ni-Mn, Co-Mn, and Mn-Mn are more in the austenite phase than in the martensite phase. This behavior results in the decrease of the martensite temperature with increasing the Co concentration [33].

When increasing the Co concentration at the Ni site(with $z = 0$) leads to a decrease in the e/a ratio and the lattice parameter(cell volume). This could be causing the T_C to increase, as tabulated in the Table (1).

Concentrations		Lattice Parameter (au)	Magnetic Moment(μ_B)						T_C (K)	e/a
x	z		Ni	Co	Mn _Y	Ga	Mn _Z	Total		
0	0	11.061	0.29	-	3.56	-0.08	-	4.08	393	7.50
0.12	0	11.047	0.31	1.07	3.50	-0.08	-	4.21	1138	7.44
0.24	0	11.032	0.33	0.95	3.45	-0.09	-	4.34	1148	7.38

Table 1: Structural, magnetic, and thermodynamic properties of NiMnGa(0,0) and NiMnGa(x ,0) system.

3.2 NiMnGa(0, z) systems

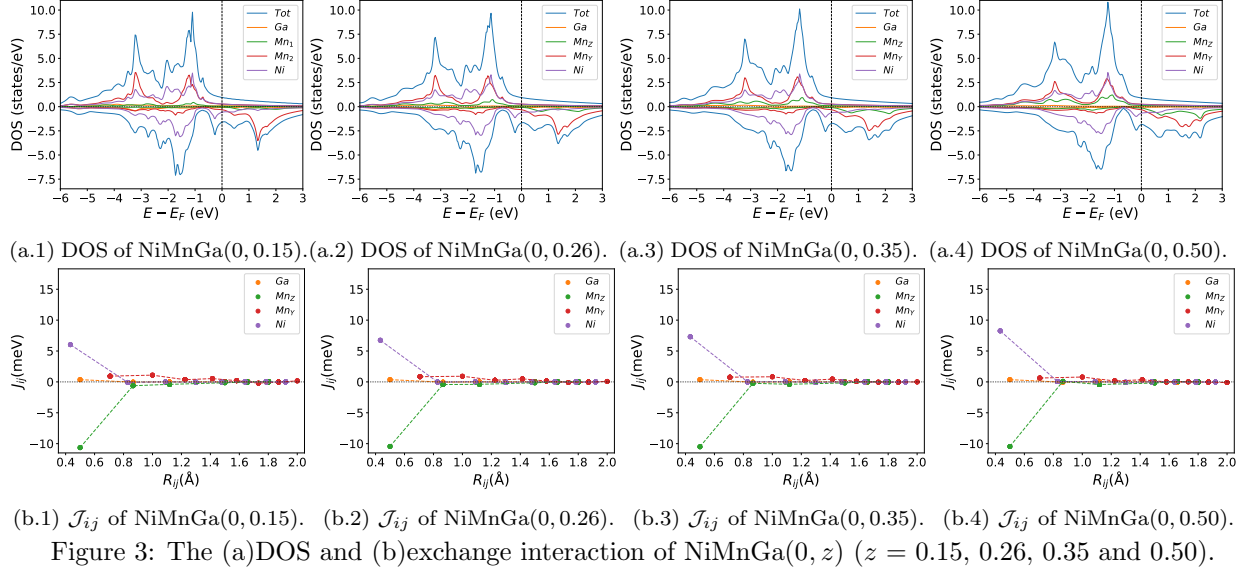
The opposite system of the one discussed in the previous section (§3.1) is NiMnGa(0, z) system, where the X site is fully ordered, but Ga is replaced by Mn, yielding Ni₂MnGa_{1- z} Mn _{z} system. The doping of Mn in the Z site, will increase the lattice parameter of the material(as shown in Figure (1d)) and induce the magnetic atom's moments as tabulated in Table (2). Notably, the moment of Ni increases up to 75% compared to the pure system, as discussed in the earlier section (§3). The Mn_Y magnetic moment increases linearly with the constant magnetic moment of Mn_Z.

The electronic structure does not change much upon doping(Figure (3a.2)), even though the absence of Co in the Ni site increases the magnetic interactions of Ni-Mn by half(Figure (3b.4)) with respect to in the case of NiMnGa(x ,0)(Figure (2b)). The most dominant interaction is Mn_Y-Mn_Z interaction, which is antiferromagnetically coupled as shown in Figure (3b) for each concentration.

Increasing the doping concentration of Mn in the Ga site(with $x = 0$), accordingly the e/a ratio starts to increase since Mn has more valence electrons compared to Ga. Additionally, the lattice parameter starts increasing and which leads to an increase in cell volume, while an increase in the Mn in the Ga site. This could be causing the T_C to start decreasing after an initial increase from the pure system. The values of the e/a ratio, lattice parameter, and T_C as tabulated in the Table (2).

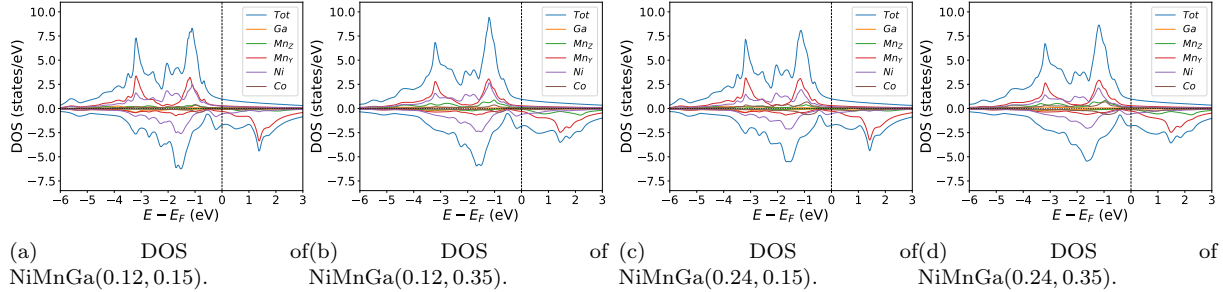
Concentrations		Lattice Parameter (au)	Magnetic Moment(μ_B)						T_C (K)	e/a
x	z		Ni	Co	Mn _Y	Ga	Mn _Z	Total		
	0.15	11.074	0.35	-	3.57	-0.08	3.65	4.76	741	7.65
0	0.26	11.084	0.40	-	3.58	-0.08	3.65	5.27	691	7.76
	0.35	11.091	0.44	-	3.59	-0.09	3.65	5.69	664	7.85
	0.50	11.101	0.51	-	3.60	-0.10	3.65	6.39	623	8.00

Table 2: Structural, magnetic and thermodynamic properties of NiMnGa(0, z) system.

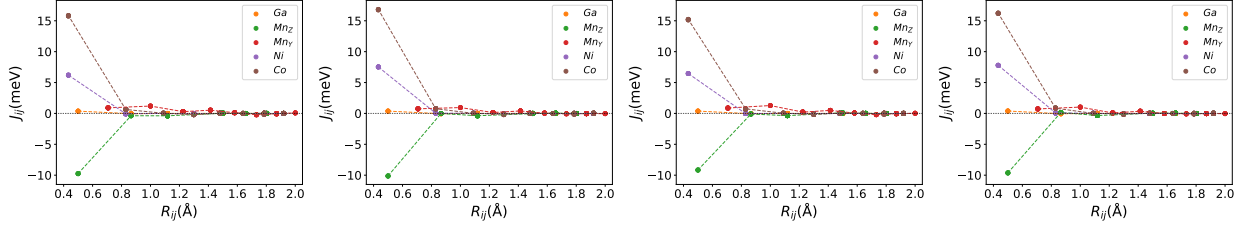


3.3 Complete disorder: NiMnGa(x, z) systems

Finally, we study the systems with disorder both at the X and Z sites, i.e., Ni $_{2-x}$ Co $_x$ MnGa $_{1-z}$ Mn $_z$. Figure (4) and Figure (5) represents the electronic and magnetic structures of NiMnGa(x, z) for ($x = 0.0, 0.12$ and 0.24) and ($z = 0.0, 0.15, 0.26, 0.35$ and 0.5).



The variation of magnetic moments of NiMnGa(x, z) are tabulated in Table (3). This doping trend shows the presence of Co at the Ni site(X position) and Mn at the Ga site(Z position), which causes the total magnetic moment to increase in accordance with the moments of all other magnetic atoms(Ni, Co and Mn $_Y$). The moment of a non-magnetic Ga atom is small and like a constant. Replacing Ga with Mn, however, has an enhanced effect



(a) \mathcal{J}_{ij} of NiMnGa(0.12, 0.15). (b) \mathcal{J}_{ij} of NiMnGa(0.12, 0.35). (c) \mathcal{J}_{ij} of NiMnGa(0.24, 0.15). (d) \mathcal{J}_{ij} of NiMnGa(0.24, 0.35). Figure 5: The Exchange interaction for a completely disordered NiMnGa(x, z) system. Figures (5a-b) shows the \mathcal{J}_{ij} of $x = 0.12$ and Figures (5c-d) shows the \mathcal{J}_{ij} of $x = 0.24$ respectively with ($z = 0.15$, and 0.35). Leftover, $z = 0.26$ and 0.5 have not been plotted for brevity.

Concentrations		Lattice Parameter (au)	Magnetic Moment(μ_B)					T_C (K)	e/a	
x	z		Ni	Co	Mn $_Y$	Ga	Mn $_Z$			Total
0.12	0.15	11.062	0.37	1.08	3.51	-0.09	3.60	4.90	1375	7.59
	0.26	11.066	0.42	1.14	3.52	-0.09	3.60	5.41	1465	7.70
	0.35	11.073	0.46	1.18	3.52	-0.09	3.59	5.82	1538	7.79
	0.50	11.082	0.52	1.26	3.54	-0.10	3.59	6.52	1653	7.94
0.24	0.15	11.042	0.39	1.08	3.46	-0.09	3.54	5.03	1389	7.53
	0.26	11.048	0.44	1.13	3.47	-0.09	3.54	5.54	1477	7.64
	0.35	11.054	0.48	1.18	3.47	-0.10	3.54	5.95	1549	7.73
	0.50	11.063	0.54	1.25	3.48	-0.10	3.54	6.63	1662	7.88

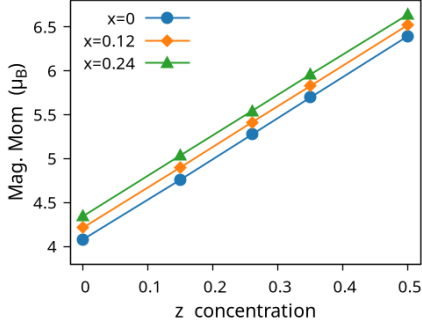
Table 3: Structural, magnetic, and thermodynamic properties of NiMnGa(x, z) system.

on the total magnetic moment. Especially, Mn $_Z = 50\%$ gives a relatively large magnetic moment compared to others.

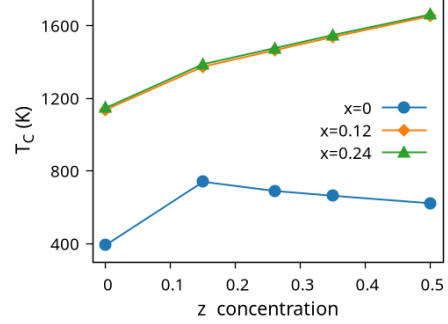
The variation of the magnetic moment of NiMnGa(x, z) as a function of doping concentration is shown in Figure (6a). The change in magnetic moment of the system is linear within the doping range. This well-behaved nature is good for tuning and applicability of this system.

In Figure (5), we have shown the exchange interactions of NiMnGa(x, z). From the figures, the ferromagnetic interactions are more dominant in the system. The competing antiferromagnetic interaction(Mn $_Z$ -Mn $_Y$) is less than the ferromagnetic interaction(Co-Mn $_Y$). Notably, the Co-Mn $_Y$ has more ferromagnetic interaction with a value above ≈ 15 meV. After initial doping of the X site, the exchange interaction energies are approximately the same for $x = 0.12$ and 0.24 , with corresponding z concentrations. This could be the cause of the relatively comparable T_C in NiMnGa(x, z).

Finally, we have done mean field-based calculations to find the T_C of the systems. Our re-



(a) Variation of magnetic moment with doping concentration.



(b) Variation of T_C with doping concentration.

Figure 6: Variation of magnetic moment and T_C of $\text{NiMnGa}(x, z)$.

sult shows that doping both X and Z sites increases the T_C . Nevertheless, for $\text{NiMnGa}(0, z)$, T_C is highest around $z = 0.15$, then it starts decreasing. On the other hand, doping a little in the X site increases the T_C steadily. Our T_C for $\text{NiMnGa}(0, 0)$ commensurate with [32, 33]. Unfortunately, we are unable to find any literature on the variation of T_C with doping. The variation of T_C is shown in Figure (6b) and tabulated in Table (1, 2, 3) for $\text{NiMnGa}(0$ and $x, 0)$, $\text{NiMnGa}(0, z)$ and $\text{NiMnGa}(x, z)$ respectively.

The e/a ratio and lattice parameter increase even in the presence of Co at the Ni site since Mn is present at the Ga site. Here, the e/a ratio and cell volume increase, however the T_C also increases since the presence of Co at the Ni site. In Table (3), we have reported the lattice parameter(au), Curie temperature(T_C), and e/a ratio values.

4 Discussions

The lattice parameter increases when Mn is doped at the Ga site ascribed to its larger atomic radius i.e., $r_{\text{Mn}}(1.61 \text{ \AA}) > r_{\text{Ga}}(1.36 \text{ \AA})$. In contrast, doping of Co at the Ni site decreases its lattice constants even though the atomic radius of Co(1.52 \AA) is larger than Ni(1.49 \AA). This can be associated with the following reasons: Firstly, the exchange interaction between the Co and Mn is higher than the Ni and Mn, and this can be well understood from Figures ((1c), (2b.1-b.2)). Secondly, the $d-d$ hybridization of Co and Mn is relatively stronger than Ni and Mn [47]. Then the lattice parameter starts to decrease as the Co concentration in the Ni site increases, as shown in Figure (1d).

In the pristine(Ni_2MnGa) DOS, we observed a pseudogap in the minority channel around $\approx 1 \text{ eV}$ below the Fermi-level. This pseudogap originated by the hybridization between $3d$ orbitals of Ni and $3p$ orbitals of Ga. The gap is terminated by a peak just below the Fermi-level originating from the hybridization of the same orbitals and drives the system to

Jahn-Teller instability. In $\text{NiMnGa}(x, 0)$ and $\text{NiMnGa}(x, z)$ systems, the doping at the Ni site stabilizes the Jahn-Teller instability as the peak smears out and the pseudogap becomes narrower with higher x value, as shown in Figure (2a) for $\text{NiMnGa}(x, 0)$ and Figure (4) for $\text{NiMnGa}(x, z)$. In $\text{NiMnGa}(0, z)$ systems the pseudogap almost remains the same throughout the doping range as shown in Figure (3a).

The magnetic moments of $\text{NiMnGa}(x, 0)$, $\text{NiMnGa}(0, z)$, and $\text{NiMnGa}(x, z)$ are shown in Table (1), Table (2), and Table (3), respectively. From the tables and Figure (6a), which shows the variation of the total magnetic moment as a function of x and z concentrations, we see the general features: (i) Magnetic moment is increasing linearly with doping. (ii) Magnetic moment increases faster by doping in Z site than doping in X site. This value is due to the overall magnetic moments of X site occupants, i.e., Ni and Co have weaker magnetic moment than Mn_Z . (iii) Mn_Z has a higher magnetic moment than the Mn_Y site. The antiferromagnetic interaction between the Mn_Y and Mn_Z atoms is stronger since the inter-atomic distance from Mn_Y to Mn_Z are smaller compared to Mn of the same sites (Mn_Y to Mn_Y , and Mn_Z to Mn_Z). The variation in x and z affects the atomic moments in various sites and the total magnetic moments. General observations are: (i) Atomistic moments of X sites are most susceptible to x and z concentrations, while Y and Z sites moments remain almost unchanged. (ii) Both Ni and Co moment increases with x, z concentration but more with z concentrations.

The Curie temperature (T_C) has been calculated using mean field approximations (MFA). As expected, MFA overestimates the T_C . For pure Ni_2MnGa , our calculated $T_C \approx 392$ K is in good agreement with experimental findings 382 K [48] (365 K is reported by [32, 33]). For $\text{NiMnGa}(x, z)$, the qualitative variation of T_C increases monotonously, with the quantitative value matching the previous findings [27]. T_C for $\text{NiMnGa}(0, z)$ first increases from 392 K to 741 K for $z = 0.15$. Higher doping of Mn_Z decreases the T_C monotonously. For Co-doped systems, both $\text{NiMnGa}(x, 0)$ and $\text{NiMnGa}(x, z)$ increase monotonously and give approximately the same T_C irrespective of Co concentrations. To get an understanding of the variation of T_C , we have calculated the magnetic pair interaction \mathcal{J}_{ij} as shown in Figures ((1c), (2b), (3b), and (5)) for Ni_2MnGa , $\text{NiMnGa}(x, 0)$, $\text{NiMnGa}(0, z)$ and $\text{NiMnGa}(x, z)$ respectively with Mn_Y at the center. When the Co atom is present, i.e., $x \neq 0$ (as in $\text{NiMnGa}(x, 0)$ and $\text{NiMnGa}(x, z)$ case), Co and Mn_Y is the dominant interaction. The difference is that for $\text{NiMnGa}(x, 0)$, the maximum interaction is almost constant (2b), but for $\text{NiMnGa}(x, z)$, the interaction keeps increasing. The same variation is evident from Figure (6b) for $x = 0.15$ and 0.24. For $\text{NiMnGa}(0, z)$, there is a ferro-antiferro competition between Ni- Mn_Y and Mn_Y - Mn_Z . This brings the T_C down after the initial increase from pure Ni_2MnGa .

5 Conclusion

We have investigated the electronic and magnetic properties of $\text{Ni}_{2-x}\text{Co}_x\text{MnGa}_{1-z}\text{Mn}_z$, with $0 \leq x \leq 0.24$, and $0 \leq z \leq 0.5$. The study of replacing both X and Z is substantially sparse compared to any one of them. We have used DFT and MFA to study the compound effect of dual-doping. Electronic structures, DOS, and magnetic properties including magnetic exchange interactions and moments are calculated using DFT as implemented in the SPRKKR package. The Curie temperature (T_C) is calculated using MFA. Our calculation shows the existence of strong Mn-Mn antiferromagnetic interaction between Mn at Ga and Mn at its sub-lattice. It is also noticed that changing concentration at Mn_Z does not change the magnetic exchange substantially. This is an interesting result, as opposed to the findings in the case of $\text{Ni}_2\text{Mn}_{1+x}\text{Sn}_{1-x}$ [34].

The T_C 's are obtained using MFA simulations using the magnetic exchange interaction values obtained from *ab-initio* calculations. The numerical results for the pure system are close to that reported by experiments.

We point out the calculations are done in cubic ($c/a = 1$) phases only. Though, in the dual-doping case, we have shown the variation of magnetic exchange interaction parameters and magnetic Curie temperatures. These findings will help to design the functional properties like MCE and shape memory alloys by alloying Ni_2MnGa suitably.

6 Acknowledgement

We acknowledge the High Performance Computing Center (HPCC), SRM IST for providing the computational facility to carry out this research work effectively.

References

- [1] T. I. R. E. A. (IRENA), Renewable energy: A key climate solution. URL <https://www.irena.org/climatechange/Renewable-Energy-Key-climate-solution>
- [2] M. Fitta, W. Sas, T. Korzeniak, Tunable critical temperature and magnetocaloric effect in ternary prussian blue analogue, J. Magn. Magn. Mater 465 (2018) 640–645. doi: 10.1016/j.jmmm.2018.06.053. URL <https://doi.org/10.1016%2Fj.jmmm.2018.06.053>
- [3] R. A. de Groot, F. M. Mueller, P. G. van Engen, K. H. J. Buschow, New class of materials: Half-metallic ferromagnets, Phys. Rev. Lett. 50 (25) (1983) 2024–2027. doi: 10.1103/physrevlett.50.2024.

- [4] S. Ishida, S. Akazawa, Y. Kubo, J. Ishida, Band theory of Co_2MnSn , Co_2TiSn and Co_2TiAl , *J. Phys. F: Met. Phys.* 12 (6) (1982) 1111–1122. doi:10.1088/0305-4608/12/6/012.
- [5] S. Fujii, S. Sugimura, Ishida, S. Asano, Hyperfine fields and electronic structures of the heusler alloys Co_2MnX ($X=\text{Al, Ga, Si, Ge, Sn}$), *J. Phys.: Condens. Matter* 2 (43) (1990) 8583–8589. doi:10.1088/0953-8984/2/43/004.
- [6] M. Jourdan, J. Minár, J. Braun, A. Kronenberg, S. Chadov, B. Balke, A. Gloskovskii, M. Kolbe, H. Elmers, G. Schönhense, H. Ebert, C. Felser, M. Kläui, Direct observation of half-metallicity in the heusler compound Co_2MnSi , *Nat. Commun.* 5 (1) (2014) 3974. doi:10.1038/ncomms4974.
- [7] K. Elphick, W. Frost, M. Samiepour, T. Kubota, K. Takanashi, H. Sukegawa, S. Mitani, A. Hirohata, Heusler alloys for spintronic devices: review on recent development and future perspectives, *Sci Technol Adv Mat* 22 (1) (2021) 235–271, PMID: 33828415. doi:10.1080/14686996.2020.1812364.
URL <https://doi.org/10.1080/14686996.2020.1812364>
- [8] S. Jiang, K. Yang, Review of high-throughput computational design of heusler alloys, *Journal of Alloys and Compounds* 867 (2021) 158854. doi:<https://doi.org/10.1016/j.jallcom.2021.158854>.
URL <https://www.sciencedirect.com/science/article/pii/S0925838821002619>
- [9] L. Wollmann, A. K. Nayak, S. S. Parkin, C. Felser, Heusler 4.0: Tunable materials, *Annu. Rev. Mater. Res.* 47 (1) (2017) 247–270. doi:10.1146/annurev-matsci-070616-123928.
URL <https://doi.org/10.1146/annurev-matsci-070616-123928>
- [10] A. Ahmad, S. Mitra, S. K. Srivastava, A. K. Das, Giant magnetocaloric effect in Co_2FeAl heusler alloy nanoparticles, *J. Phys. D: Appl. Phys.* 54 (38) (2021) 385001. doi:10.1088/1361-6463/ac0aba.
URL <https://doi.org/10.1088/1361-6463/ac0aba>
- [11] X. Yang, Y. Wang, M. Du, Y. Xue, First-principles study of Pt doping effects on Ni_2MnGa and Ni_2FeGa ferromagnetic shape memory alloys, *Journal of Applied Physics* 126 (8) (2019) 085103. arXiv:<https://doi.org/10.1063/1.5116247>, doi:10.1063/1.5116247.
URL <https://doi.org/10.1063/1.5116247>

- [12] L. Bainsla, A. I. Mallick, M. M. Raja, A. A. Coelho, A. K. Nigam, D. D. Johnson, A. Alam, K. G. Suresh, Origin of spin gapless semiconductor behavior in CoFeCrGa: Theory and experiment, *Phys. Rev. B* 92 (2015) 045201. doi:10.1103/PhysRevB.92.045201.
URL <https://link.aps.org/doi/10.1103/PhysRevB.92.045201>
- [13] A. Kundu, S. Ghosh, R. Banerjee, S. Ghosh, B. Sanyal, New quaternary half-metallic ferromagnets with large curie temperatures, *Sci. Rep.* 7 (1) (2017) 1803. doi:10.1038/s41598-017-01782-5.
- [14] T. Kihara, T. Roy, X. Xu, A. Miyake, M. Tsujikawa, H. Mitamura, M. Tokunaga, Y. Adachi, T. Eto, T. Kanomata, Observation of inverse magnetocaloric effect in magnetic-field-induced austenite phase of heusler alloys $\text{Ni}_{50-x}\text{Co}_x\text{Mn}_{31.5}\text{Ga}_{18.5}$ ($x=9$ and 9.7), *Phys. Rev. Materials* 5 (2021) 034416. doi:10.1103/PhysRevMaterials.5.034416.
URL <https://link.aps.org/doi/10.1103/PhysRevMaterials.5.034416>
- [15] J. Liu, N. Scheerbaum, S. Kauffmann-Weiss, O. Gutfleisch, NiMn-based alloys and composites for magnetically controlled dampers and actuators, *Adv Eng Mater* 14 (8) (2012) 653–667. doi:10.1002/adem.201200038.
- [16] R. Mahat, S. KC, U. Karki, J. Y. Law, V. Franco, I. Galanakis, A. Gupta, P. LeClair, Possible half-metallic behavior of $\text{Co}_{2-x}\text{Cr}_x\text{FeGe}$ heusler alloys: Theory and experiment, *Phys. Rev. B* 104 (2021) 014430. doi:10.1103/PhysRevB.104.014430.
URL <https://link.aps.org/doi/10.1103/PhysRevB.104.014430>
- [17] Z. Guan, J. Bai, J. Gu, X. Liang, D. Liu, X. Jiang, R. Huang, Y. Zhang, C. Esling, X. Zhao, L. Zuo, First-principles investigation of B2 partial disordered structure, martensitic transformation, elastic and magnetic properties of all-d-metal Ni-Mn-Ti heusler alloys, *Journal of Materials Science and Technology* 68 (2021) 103–111. doi:<https://doi.org/10.1016/j.jmst.2020.08.002>.
URL <https://www.sciencedirect.com/science/article/pii/S1005030220306940>
- [18] V. G. de Paula, M. S. Reis, All-d-metal full heusler alloys: A novel class of functional materials, *Chemistry of Materials* 33 (14) (2021) 5483–5495. arXiv:<https://doi.org/10.1021/acs.chemmater.1c01012>, doi:10.1021/acs.chemmater.1c01012.
URL <https://doi.org/10.1021/acs.chemmater.1c01012>
- [19] F. Heusler, Ueber magnetische manganlegierungen, *Phys. Ges* 12 (219) (1903).

- [20] F. Heusler, W. Starck, E. Haupt, Magnetisch-chemische studien, Phys. Ges 5 (220) (1903).
- [21] E. T. Dilmieva, Y. S. Koshkid'ko, V. V. Koledov, A. P. Kamantsev, A. V. Mashirov, J. Cwik, V. V. Khovaylo, V. G. Shavrov, Formation of a martensitic twins structure in $\text{Ni}_{2.16}\text{Mn}_{0.84}\text{Ga}$ heusler alloy by high magnetic fields under adiabatic and isothermal conditions, Bull. Russ. Acad. Sci.: Phys. 81 (11) (2017) 1283–1288. doi:[10.3103/s1062873817110077](https://doi.org/10.3103/s1062873817110077).
- [22] C. Seguí, E. Cesari, Ordering mechanism and kinetics in $\text{Ni}_2\text{Mn}_{1-x}\text{Cu}_x\text{Ga}$ ferromagnetic shape memory alloys, Journal of Alloys and Compounds 887 (2021) 161302. doi:<https://doi.org/10.1016/j.jallcom.2021.161302>.
URL <https://www.sciencedirect.com/science/article/pii/S0925838821027110>
- [23] A. P. Kamantsev, V. V. Koledov, A. V. Mashirov, E. T. Dilmieva, V. G. Shavrov, J. Cwik, A. S. Los, V. I. Nizhankovskii, K. Rogacki, I. S. Tereshina, Y. S. Koshkid'ko, M. V. Lyange, V. V. Khovaylo, P. Ari-Gur, Magnetocaloric and thermomagnetic properties of $\text{Ni}_{2.18}\text{Mn}_{0.82}\text{Ga}$ heusler alloy in high magnetic fields up to 140 kOe, J Appl Phys 117 (16) (2015) 163903. doi:[10.1063/1.4918914](https://doi.org/10.1063/1.4918914).
- [24] Franco, V., Blázquez, J.S., Ingale, B., C. A., The magnetocaloric effect and magnetic refrigeration near room temperature: Materials and models, Annu. Rev. Mater. Res. 42 (1) (2012) 305–342. doi:[10.1146/annurev-matsci-062910-100356](https://doi.org/10.1146/annurev-matsci-062910-100356).
URL <https://doi.org/10.1146/annurev-matsci-062910-100356>
- [25] R. Y. Umetsu, X. Xu, R. Kainuma, NiMn-based metamagnetic shape memory alloys, Scr. Mater. 116 (2016) 1–6. doi:[10.1016/j.scriptamat.2016.01.006](https://doi.org/10.1016/j.scriptamat.2016.01.006).
- [26] A. Okubo, X. Xu, R. Y. Umetsu, T. Kanomata, K. Ishida, R. Kainuma, Magnetic properties of $\text{Co}_{50-x}\text{Ni}_x\text{Mn}_{25}\text{Al}_{25}$ alloys with B2 structure, J Appl Phys 109 (7) (2011) 07B114. doi:[10.1063/1.3559536](https://doi.org/10.1063/1.3559536).
- [27] T. Kanomata, Y. Kitsunai, K. Sano, Y. Furutani, H. Nishihara, R. Y. Umetsu, R. Kainuma, Y. Miura, M. Shirai, Magnetic properties of quaternary heusler alloys $\text{Ni}_{2-x}\text{Co}_x\text{MnGa}$, Phys. Rev. B 80 (2009) 214402. doi:[10.1103/PhysRevB.80.214402](https://doi.org/10.1103/PhysRevB.80.214402).
URL <https://link.aps.org/doi/10.1103/PhysRevB.80.214402>
- [28] Uijttewaal, M. A., Hickel, T., Neugebauer, J., Gruner, M. E., E. P., Understanding the phase transitions of the Ni_2MnGa magnetic shape memory system from first principles, Phys. Rev. Lett. 102 (2009) 035702. doi:[10.1103/PhysRevLett.102.035702](https://doi.org/10.1103/PhysRevLett.102.035702).
URL <https://link.aps.org/doi/10.1103/PhysRevLett.102.035702>

- [29] S. Singh, B. Dutta, S. W. D'Souza, M. G. Zavareh, P. Devi, A. S. Gibbs, T. Hickel, S. Chadov, C. Felser, D. Pandey, Robust bain distortion in the premartensite phase of a platinum-substituted Ni_2MnGa magnetic shape memory alloy, *Nat. Commun.* 8 (2017) 1006. doi:<https://doi.org/10.1038/s41467-017-00883-z>.
- [30] V. D. Buchelnikov, V. V. Sokolovskiy, Magnetocaloric effect in Ni-Mn-X (X = Ga, In, Sn, Sb) heusler alloys, *The Physics of Metals and Metallography* 112 (7) (2011) 633–665. doi:10.1134/s0031918x11070052.
- [31] R. Kainuma, Y. Imano, W. Ito, H. Morito, Y. Sutou, K. Oikawa, A. Fujita, K. Ishida, S. Okamoto, O. Kitakami, T. Kanomata, Metamagnetic shape memory effect in a heusler-type $\text{Ni}_{43}\text{Co}_7\text{Mn}_{39}\text{Sn}_{11}$ polycrystalline alloy, *Appl. Phys. Lett.* 88 (19) (2006) 192513. doi:10.1063/1.2203211.
- [32] F. Orlandi, A. Çakır, P. Manuel, D. D. Khalyavin, M. Acet, L. Righi, Neutron diffraction and symmetry analysis of the martensitic transformation in Co-doped Ni_2MnGa , *Phys. Rev. B* 101 (2020) 094105. doi:10.1103/PhysRevB.101.094105. URL <https://link.aps.org/doi/10.1103/PhysRevB.101.094105>
- [33] V. Sokolovskiy, A. Grünebohm, V. Buchelnikov, P. Entel, Ab initio and monte carlo approaches for the magnetocaloric effect in Co and In-doped Ni-Mn-Ga heusler alloys, *Entropy* 16 (9) (2014) 4992–5019. doi:10.3390/e16094992.
- [34] V. V. Sokolovskiy, V. D. Buchelnikov, M. A. Zagrebin, P. Entel, S. Sahoo, M. Ogura, First-principles investigation of chemical and structural disorder in magnetic $\text{Ni}_2\text{Mn}_{1+x}\text{Sn}_{1-x}$ heusler alloys, *Phys. Rev. B* 86 (2012) 134418. doi:10.1103/PhysRevB.86.134418. URL <https://link.aps.org/doi/10.1103/PhysRevB.86.134418>
- [35] Z. Ni, X. Guo, Q. Li, Z. Liang, H. Luo, F. Meng, Effect of Zn-doping on the phase transition and magnetic properties of heusler alloys $\text{Ni}_2\text{MnGa}_{1-x}\text{Zn}_x$ ($x=0, 0.25, 0.5, 0.75$ and 1), *Journal of Magnetism and Magnetic Materials* 464 (2018) 65–70. doi:<https://doi.org/10.1016/j.jmmm.2018.05.044>. URL <https://www.sciencedirect.com/science/article/pii/S0304885318307790>
- [36] M. Halder, K. Suresh, Effect of Fe substitution at the Ni and Mn sites on the magnetic properties of $\text{Ni}_{50}\text{Mn}_{35}\text{In}_{15}$ heusler alloys, *Journal of Alloys and Compounds* 647 (2015) 310–314. doi:<https://doi.org/10.1016/j.jallcom.2015.06.121>. URL <https://www.sciencedirect.com/science/article/pii/S0925838815302383>

- [37] P. Cao, F. Tian, W. Li, L. Vitos, Y. Wang, Ideal superelasticity in Ni-based heusler alloys, *Acta Materialia* 210 (Mar 2021). doi:10.1016/j.actamat.2021.116816.
- [38] R. Banerjee, A. Mookerjee, Augmented space recursion code and application in simple binary metallic alloy, *Int. J. Modern Phys. C* 21 (02) (2010) 205–220. doi:10.1142/s0129183110015051.
- [39] H. Ebert, D. Ködderitzsch, J. Minár, Calculating condensed matter properties using the KKR-Green's function method—recent developments and applications, *Reports on Progress in Physics* 74 (9) (2011) 096501. doi:10.1088/0034-4885/74/9/096501.
- [40] H. Ebert, Fully relativistic band structure calculations for magnetic solids - formalism and application, in: H. Dreyssé (Ed.), *Electronic Structure and Physical Properties of Solids*, Springer Berlin Heidelberg, Berlin, Heidelberg, 2000, pp. 191–246.
- [41] P. N. Mavropoulos Phivos, The Korringa-Kohn-Rostoker (KKR) Green Function Method I. Electronic Structure of Periodic Systems, in: D. M. J. Grotendorst, S. Blügel (Ed.), *Computational Nanoscience: Do It Yourself!*, 2006.
- [42] J. P. Perdew, K. Burke, M. Ernzerhof, Generalized Gradient Approximation Made Simple, *Phys. Rev. Lett.* 77 (18) (1996) 3865–3868. doi:10.1103/physrevlett.77.3865.
URL <https://doi.org/10.1103%2Fphysrevlett.77.3865>
- [43] A. Jain, S. P. Ong, G. Hautier, W. Chen, W. D. Richards, S. Dacek, S. Cholia, D. Gunter, D. Skinner, G. Ceder, K. A. Persson, Commentary: The materials project: A materials genome approach to accelerating materials innovation, *APL Materials* 1 (1) (2013) 011002. doi:10.1063/1.4812323.
URL <https://doi.org/10.1063%2F1.4812323>
- [44] A. Liechtenstein, M. Katsnelson, V. Antropov, V. Gubanov, Local spin density functional approach to the theory of exchange interactions in ferromagnetic metals and alloys, *J. Magn. Magn. Mater* 67 (1) (1987) 65–74. doi:[https://doi.org/10.1016/0304-8853\(87\)90721-9](https://doi.org/10.1016/0304-8853(87)90721-9).
URL <https://www.sciencedirect.com/science/article/pii/0304885387907219>
- [45] M. B. Sahariah, S. Ghosh, C. S. Singh, S. Gowtham, R. Pandey, First-principles computation of structural, elastic and magnetic properties of Ni₂FeGa across the martensitic transformation, *J. Phys.: Condens. Matter* 25 (2) (2012) 025502. doi:10.1088/0953-8984/25/2/025502.

- [46] S. Ghosh, B. Sanyal, Complex magnetic interactions in off-stoichiometric NiMnGa alloys, *Journal of Physics: Condensed Matter* 22 (34) (2010) 346001. doi:10.1088/0953-8984/22/34/346001.
URL <https://doi.org/10.1088/0953-8984/22/34/346001>
- [47] T. Chang-Long, J. Jiu-Xing, T. X. Hua, C. Wei, Effect of Co on magnetic property and phase stability of Ni-Mn-Ga ferromagnetic shape memory alloys: A first-principles study, *Chinese Physics B* 19 (10) (2010) 107102.
- [48] A. U. Saleheen, J.-H. Chen, D. P. Young, I. Dubenko, N. Ali, S. Stadler, Critical behavior in Ni₂MnGa and Ni₂Mn_{0.85}Cu_{0.15}Ga, *J Appl Phys* 123 (20) (2018) 203904. doi:10.1063/1.5025196.
URL <https://doi.org/10.1063/1.5025196>